

Tuning Magnetic Properties of Thick CoFeB Film by Interlayer Coupling in Trilayer Structured Thin Films

Anabil Gayen¹, Kosuri Umadevi², Arout Chelvane J² and Perumal Alagarsamy^{1*}

¹Department of Physics, Indian Institute of Technology Guwahati, Guwahati-781039, India

²Defence Metallurgical Research Laboratory, Hyderabad-500058, India

Abstract

This study deals with tuning magnetic properties of a thick amorphous (a-)Co₂₀Fe₆₀B₂₀ (CoFeB262) film by using interlayer magnetic coupling in trilayer structured films of [CoFeB262 (100 nm)/Cr,Ta (x nm)]/CoFeB262 (y nm) with y=2-50, x_{Cr}=0.75, 2 and x_{Ta}=1, 4. All the films are deposited directly on thermally oxidized Si substrate at ambient temperature using magnetron sputtering. The as-deposited a-CoFeB262 (100 nm) film exhibits magnetic stripe domain and transcritical hysteresis loop due to large effective magnetic anisotropy caused by stress induced during deposition of the films. On the other hand, the shape of magnetic hysteresis (M-H) loops in trilayer films transforms from transcritical to rectangular shaped one with enhanced remanence ratio (M_r/M_s) of ≥ 75% and single magnetization reversal behavior. This effectively reduces coercivity (H_c) and field required to saturate magnetization (H_s) in trilayer films. However, the changes in the loop shape and reductions in H_c and H_s depend strongly on x and y. Magnetic domain images obtained using Kerr microscopy in trilayer films show a rapid switching of large-sized domains along easy-axis and weak ripple domains along hard-axis. In addition, the magnetization reversal behavior along the hard-axis strongly depends on x_(Cr,Ta). M-H loops obtained at different temperatures between 30 K and 300 K reveal no change in loop shape for trilayer films with small x and y, while the disappearance of shearing and formation of additional steps at low temperatures are observed for films with large x and y. The observed results are explained on the basis of change in interlayer coupling between CoFeB262 layers with x, y and temperature. Furthermore, these results clearly confirm that the magnetic properties of thick CoFeB262 film with stripe domain can easily be tuned into in-plane magnetization by this simple trilayer structured thin films.

Keywords: Thin films; Magnetic properties; Interlayer coupling; Magnetic anisotropy; Stripe domain; Magnetization reversal

Introduction

Magnetic thin films with enhanced soft magnetic properties, simple magnetic domain structure and reduced media noise are enormously required in areas like magnetic recording, communication devices, automotive industry, and other modern magneto-electronic devices. In these applications, the ferromagnetic thin films are used as either magnetic flux guide or magnetic flux amplifier in high-frequency applications, provided these magnetic films exhibit a simple magnetic domain structure with the magnetization oriented in a particular direction [1-5]. Hence, over last two decades extensive studies have been carried out on various types of magnetic thin films [HITPERM, CoFeB, CoNbFe, Co(Ta,Nb,Fe)Zr, FeAlSi, FeBSi, FeCuNbSiB, Fe(Co)TaN, FeTaC, etc.] in both single-layer and multilayer forms to improve the soft magnetic properties [6-14]. Among these films, amorphous (a-)CoFeB thin film is found to be one of the promising materials suitable for various applications due to its tunable magnetic properties. A detailed review of the literature reveals that the magnetic properties of the CoFeB films are strongly dependent on its thickness (t): (i) Ultrathin CoFeB (t<5 nm) films display a strong perpendicular magnetic anisotropy ranging between 0.5 × 10⁶ J/m³ and 2 × 10⁶ J/m³ mainly originated from the interfacial effects [15-17]. As a result, these ultrathin films find applications in magnetic tunnel junctions, magnetic random access memory, spin logic based devices and various other spintronics based applications [15,16,18-26]. (ii) With increasing t>5 nm, CoFeB films exhibit in-plane magnetic anisotropy induced by the formation of aligned ferromagnetic atom pairs during deposition process for t up to 50 nm [27]. (iii) On further increasing t above 50 nm, the stress induced magnetic anisotropy overcomes in-plane anisotropy and increases the degree of local disorder in the easy-axis of the as-deposited films [28]. This leads to the formation of random magnetic anisotropy with a negative influence on the soft magnetic properties

at higher t and induces magnetic stripe domains. Therefore, thicker CoFeB films become magnetically hard and display transcritical loop.

In order to control the development of random magnetic anisotropy, complex magnetic domain structure at larger t and to improve soft magnetic properties with simple domain structure, tunable anisotropy (K_u), coercivity (H_c) and low applied field for magnetization saturation (H_s), the most commonly adopted approaches are (i) to fabricate the multilayer structured thin films having ferromagnetic layers separated by non-magnetic (metallic and non-metallic) layers [7-11,29] and (ii) to execute controlled heat treatment of the amorphous precursor under different annealing environments [30]. For instance, Feng et al. [31,32] reported spacer layer materials and its thickness dependence of soft magnetic properties, where H_c decreases with increasing spacer layer thickness (x). Similarly, Mishra et al. [33] and Camelia et al. [34] reported that the soft magnetic properties of ferromagnetic layers beyond critical thickness are enhanced by fabricating multilayer thin films with more number of multilayers (N) and different x. Nevertheless, with increasing N, (i) the number of interfaces increases, (ii) the interlayer coupling between the ferromagnetic layers becomes complex due to increased number of interfaces [35,36], (iii) the nature and strength of magnetic coupling between ferromagnetic layers vary indiscriminately with

*Corresponding author: Perumal Alagarsamy, Department of Physics, Indian Institute of Technology Guwahati, Guwahati-781 039, India, Tel: +91-361-2582714; E-mail: alagarsamy.perumal@gmail.com

Received March 11, 2018; Accepted March 27, 2018; Published April 07, 2018

Citation: Gayen A, Umadevi K, Chelvane JA, Alagarsamy P (2018) Tuning Magnetic Properties of Thick CoFeB Film by Interlayer Coupling in Trilayer Structured Thin Films. J Material Sci Eng 7: 437. doi: [10.4172/2169-0022.1000437](https://doi.org/10.4172/2169-0022.1000437)

Copyright: © 2018 Gayen A, et al. This is an open-access article distributed under the terms of the Creative Commons Attribution License, which permits unrestricted use, distribution, and reproduction in any medium, provided the original author and source are credited.

spacer layer material and its thickness and (iv) the roughness associated with the number of interfaces increases and the average magnetization of the films decreases. Although the post heat treatment of amorphous precursor provides excellent soft magnetic properties with high Curie temperature [11,37], H_C increases progressively with increasing heat treatment temperature in the multilayer films [38-40]. As a result, the magnetic properties and magnetization reversal behaviors are highly modified [41-46].

While most of the earlier works on CoFeB films have been focused mainly on controlling the perpendicular magnetic anisotropy [15,16,19,25,26] from applications point of view, there are only limited reports available on tuning the magnetic properties of thick a-Co₂₀Fe₆₀B₂₀ (CoFeB262) based films for other possible applications such as flux guide, flux amplifiers, etc. [27,34,47,48] and from fundamental point of view. Hence, we report here an alternative approach of fabricating simple trilayer structured films of [CoFeB262 (100 nm)]/[Cr, Ta (x nm)]/CoFeB262 (y nm)], as schematically shown in Figure 1, to tune the magnetic properties of thick a-CoFeB262 (100 nm) single-layer film exhibiting stripe domain structure. These trilayer films are fabricated and characterized mainly (i) to study the effect of top CoFeB262 layer thickness on the magnetic properties of thick CoFeB262 bottom layer through different spacer layer materials (Cr and Ta), (ii) to investigate the variation in magnetic interactions between two CoFeB262 layers for various x, (iii) to understand the effect of temperature (T) on the magnetic interactions between CoFeB262 layers and (iv) to explore the possibility of tuning the magnetic properties of thick a-CoFeB262 (100 nm) film using the proposed simple trilayer structure.

Materials and Methods

Amorphous CoFeB262 (100 nm) single-layer film and trilayer films of [CoFeB262 (100 nm)]/[Cr, Ta (x nm)]/CoFeB262 (y nm)] with y=2, 5, 10, 30 and 50 nm, x_{Cr} =0.75, 2 nm and x_{Ta} =1, 4 nm were prepared using magnetron sputtering technique. All the films were deposited directly on the thermally oxidized Si substrate at ambient temperature. The base pressure of the chamber was maintained to be better than 1×10^{-4} Pa. The working gas pressure for the deposition of CoFeB262, Cr and Ta was fixed at 10 mTorr. The deposition rate of the films was pre-calibrated using *ex-situ* surface profilometer (Veeco, Dektak-150 model). The total thickness of each film in single-layer and trilayer films was controlled by monitoring the deposition time during the film deposition.

Amorphous nature of all the as-deposited CoFeB262 films was confirmed by X-ray diffraction (XRD) obtained using a high-power X-ray diffractometer (Rigaku TTRAX III, 18 kW) with Cu-K α radiation ($\lambda=1.54056$ Å) and transmission electron microscopy (TEM, JEOL 2100 and Technai G² F20) techniques. Room temperature and temperature dependent magnetic properties of the films were analyzed using vibrating sample magnetometer (VSM, LakeShore Model 7410) by performing magnetic hysteresis loops (M-H) at room temperature and at low temperatures in the temperature range between 30 K and 300 K. Magnetic domain images and Kerr loops were obtained using magneto-optic Kerr effect (MOKE) microscopy (Evico Magnetics Ltd, Germany) technique. Imaging was performed using linearly polarized light with Xenon lamp as source. Magnetic domain images were observed in both branches of hysteresis cycle in longitudinal MOKE mode. Hysteresis accompanied by simultaneous imaging has been performed for magnetic fields applied along various in-plane directions [easy (0°) and hard (90°) axes]. Simultaneous atomic force microscopy (AFM) and magnetic force microscopy (MFM) studies were performed to study the topographic feature and local magnetic domains (Bruker

Dimension Icon). MFM was performed in dual-pass lifting mode with commercially available CoCr-coated tips, which were magnetized perpendicular to the surface of the material and therefore sensitive to stray field gradients from out-of-plane oriented domains or the out-of-plane components of domains oblique to the surface. The domain images were acquired at the zero-field state.

Results and Discussions

Figure 2 shows typical XRD pattern, bright-field TEM image, selected area electron diffraction (SAED) pattern, high-resolution TEM (HRTEM) image and AFM topography of the as-deposited single-layer CoFeB262 (100 nm) thick film. It is clearly seen that as-deposited film exhibits only a broad peak at around $2\theta=44^\circ$ without any sharp peaks peculiar to any other crystalline phases. The XRD peak observed

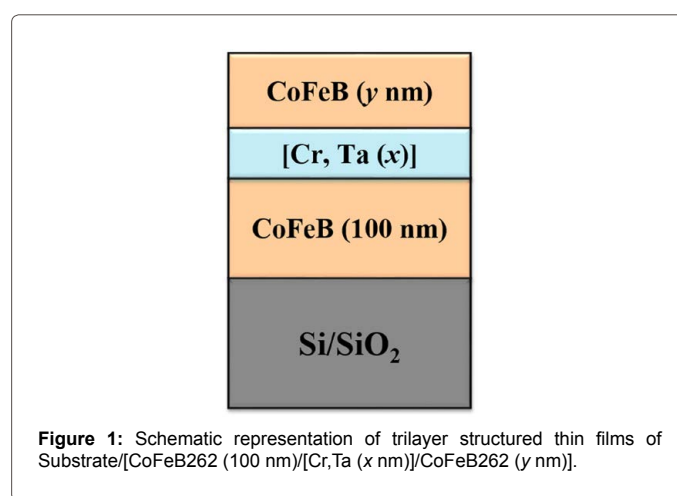


Figure 1: Schematic representation of trilayer structured thin films of Substrate/[CoFeB262 (100 nm)]/[Cr, Ta (x nm)]/CoFeB262 (y nm)].

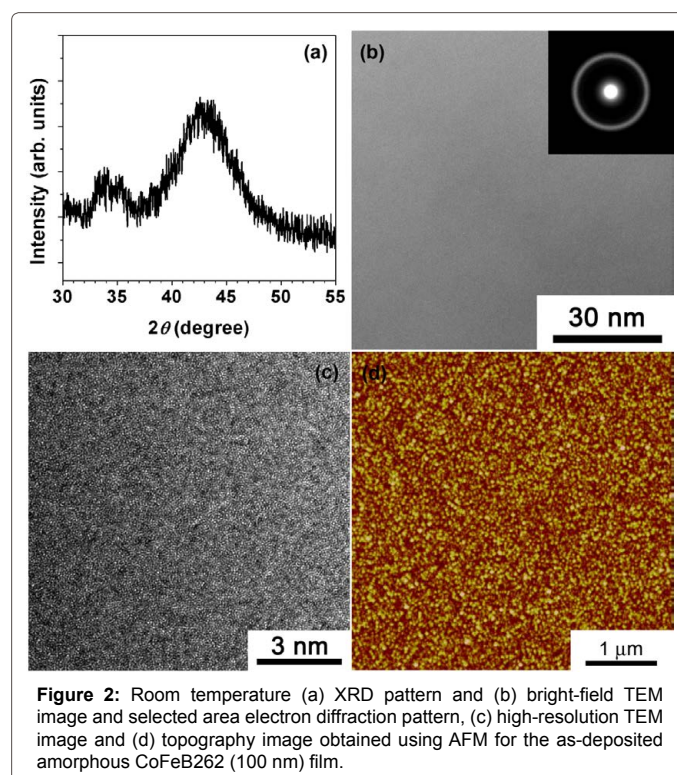


Figure 2: Room temperature (a) XRD pattern and (b) bright-field TEM image and selected area electron diffraction pattern, (c) high-resolution TEM image and (d) topography image obtained using AFM for the as-deposited amorphous CoFeB262 (100 nm) film.

at $2\theta=33.05^\circ$ represents Si(200) peak due to thermally oxidized Si substrate [49]. The amorphous nature is also confirmed from bright-field TEM image, SAED pattern and HRTEM image, which revealed the existence of plane and even contrast microstructure without any local lattice fringes and halo diffraction ring, respectively. AFM topography displays the existence of very fine and sparsely dispersed nanosized grains of size ranging between 11 and 15 nm in the as-deposited films. In addition, the film exhibits a very clear uniform surface and the average roughness of the surface is found to be between 0.4 nm and 0.7 nm.

Figure 3 depicts room temperature $M-H$ loop measured along the film plane and magnetic domain structure of the as-deposited CoFeB262 (100 nm) single-layer film. It is clearly evident that the $M-H$ loop is constituted by two different magnetization reversal processes before saturation: (a) in-plane magnetic component, which reverses quickly at fields close to H_C and (b) perpendicular component, which rotates progressively under the application of magnetic field. The latter one gives rise to almost a linear-like variation of magnetization before saturation and also requires a large applied magnetic field (H_s) of more than 1400 Oe to saturate film's magnetization. This type of hysteresis behavior with low remanence ratio ($M_R/M_S \sim 0.38$, where M_R is remnant magnetization and M_S is saturation magnetization) is called as transcritical loop [29,33,34,47,48,50-53], which is generally correlated to increase in effective magnetic anisotropy caused by the stress induced during the deposition of the films at a higher deposition rate to form amorphous structure. In addition, this leads to the formation of magnetic stripe domain pattern in thick a-CoFeB262 films, as obtained and demonstrated in Figure 3b. The width of the stripe domains determined by a proper Fast Fourier Transform analysis of the MFM image is found to be about 135 nm, which is in good agreement with the earlier reports on similar amorphous systems [47,48,50-53].

To study the effects of trilayer structures, spacer layer materials with different thicknesses (x) and thickness of the top CoFeB262 layers (y) on the room temperature magnetic properties of the thick CoFeB262 (100 nm) film, the room temperature $M-H$ loops are measured along the film plane for the trilayer films and shown in Figure 4. Figure 5 depicts the extracted parameters, such as H_C , H_s and M_R/M_S , plotted as a function of y for different x . For [CoFeB262 (100 nm)/Cr (x nm)/CoFeB262 (y nm)] films; (i) the shape of the $M-H$ loop is observed to be transcritical for the film with $y=0$. (ii) On the other hand, the introduction of top CoFeB262 film changes the nature of $M-H$ loops drastically and all the trilayer films exhibit simple $M-H$ loops with enhanced M_R/M_S and single magnetization reversal at H_C (Figure 4a). (iii) For instance, the introduction of even a thin top CoFeB262 layer ($y=2$ nm, $x_{Cr}=0.75$ nm) changes the loop shape drastically from

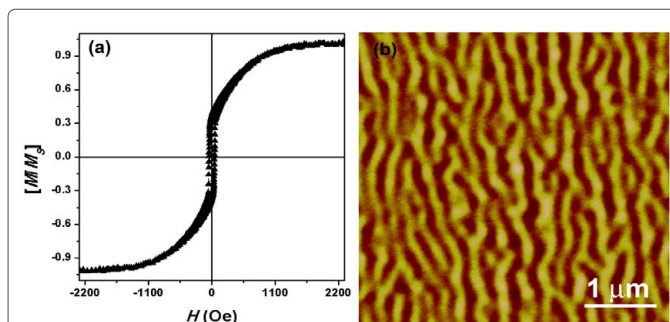


Figure 3: Room temperature (a) $M-H$ loop measured along the film plane and (b) MFM domain image for CoFeB262 (100 nm) film.

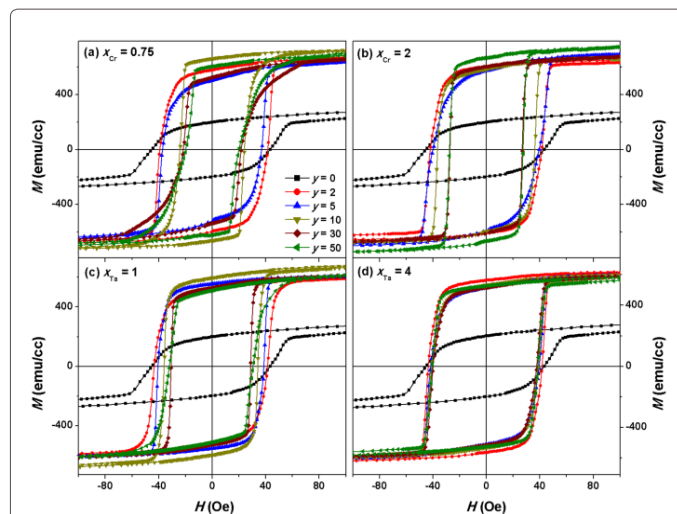


Figure 4: Room temperature $M-H$ loops measured along the film plane for trilayer films with (a) $x_{Cr}=0.75$, (b) $x_{Cr}=2$, (c) $x_{Ta}=1$ and (d) $x_{Ta}=4$ and different values of y .

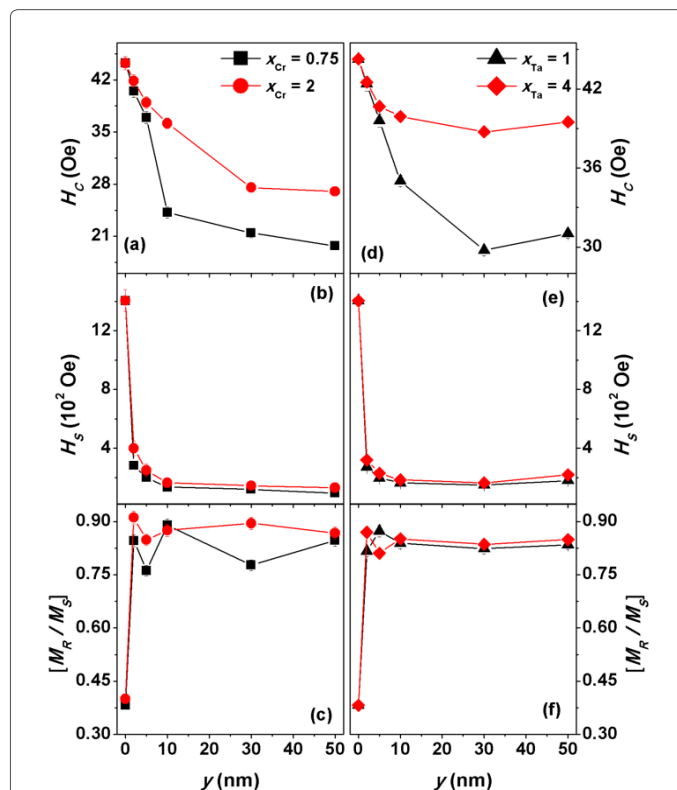


Figure 5: The variations of H_C , H_s and M_R/M_S as a function of y for trilayer films with different spacer layer materials.

transcritical into rectangular shaped loop and fades away the linear variation of magnetization before the saturation of magnetization. This certainly reduces H_s drastically from 1405 Oe to 285 Oe and enhances M_R/M_S from 0.38 to 0.85 (Figure 5b and 5c). (iv) With increasing y up to 10 nm, the rectangular shaped loops hold along with progressive reduction in H_C . (v) On further increasing $y > 10$ nm, the nature of magnetization reversal varies gradually with unfavorable shearing of

the loop, i.e., a rapid fall in magnetization followed by a long-tailed loop before saturation. In addition, M_R/M_S varies sluggishly and H_S decreases slowly. (vi) H_C decreases almost linearly at a rate of 1.98 Oe/nm with increasing y up to 10 and then the rate of decrease in H_C decreases to 0.12 Oe/nm with the further increase in y from 10 to 50 nm (Figure 5a). (vii) With increasing x_{Cr} to 2 nm, the change in the loop shape is found to be different. In contrast to $x_{Cr}=0.75$ films, no sheared loops are observed for films with $x_{Cr}=2$ and $y>10$. (viii) But, the magnitude of reduction in H_C decreases considerably. Similarly, for [CoFeB262 (100 nm)/Ta (x nm)/CoFeB262 (y nm)] films; (i) the shape of the $M-H$ loops changes drastically with the introduction of top CoFeB262 layer and all the trilayer films exhibit simple $M-H$ loops with enhanced M_R/M_S and single magnetization reversal at H_C . (ii) With increasing x_{Ta} from 1 to 4 nm, the shape of the loops is observed to be merely the same with a small reduction in H_C for films with different y . This provides almost similar $M-H$ loops for films with $x_{Ta}=4$ nm and $y=2-50$ nm. In addition, these films with different x_{Ta} do not show any sheared loops for any values of y .

The observed changes in the magnetic properties of the trilayer films as compared to single-layer film can be explained based on the nature of coupling between the CoFeB262 films through spacer layers. Generally, the interlayer coupling between two ferromagnetic layers originates from (i) the direct exchange coupling between ferromagnetic layers through pinholes in thin spacer layer [54], (ii) indirect exchange coupling through the conduction electrons of the spacer layer [Ruderman–Kittel–Kasuya–Yosida (RKKY)] [55], (iii) the magnetostatic coupling induced by the correlated interfacial roughness, also known as orange peel coupling or Néel coupling as shown in Figure 6a [42,56] and (iv) the magnetostatic coupling through stray fields of domain walls (Figure 6b) [41,57,58], and (v) the magnetostatic coupling through the magnetic poles at the edges of the films [59,60]. The single-layer film of a-CoFeB262 (100 nm) showed the transcritical loop due to the existence of in-plane and perpendicular magnetic components, which formed stripe domain structure. The introduction of even a thin top CoFeB262 layer with $x_{Cr}=0.75$ nm changed the nature of $M-H$ loop from transcritical into rectangular shaped loop. These results and the surface roughness of the bottom CoFeB262 layer suggest that the interlayer coupling due to the direct ferromagnetic coupling through pinholes and the indirect exchange coupling through RKKY interaction depends strongly on x . Since the average surface roughness of the bottom CoFeB262 (100 nm) layer is observed to be between 0.4 nm

and 0.7 nm, the growth of the subsequent Cr space layer with $x_{Cr}=0.75$ nm on top of thick CoFeB262 layer may not be continuous all the way and therefore the top CoFeB262 layer may not be well separated from the bottom CoFeB262 layer perfectly. As a result, there exists a direct exchange coupling between CoFeB262 layers at random locations depending on the roughness. This arrangement helps to switch the CoFeB262 layers collectively and displays simple loop. However, with increasing $y>10$, the rectangular shaped loop changed into sheared loop with long tailing. Navas et al. [36] reported thickness dependent slow approach to saturation in CoCrPt films and attributed to the existence of small bubble domains that are magnetostatically stabilized by the surrounding regions [61]. Similarly, Park et al. [35] reported that with increasing N in $(Co/Pt)_N$ films, the shape of the $M-H$ loops deviated away from perfect rectangular shape to sheared loop with long-tailing. This was correlated to the inherited increase in interface roughness accompanied with increasing the film thickness since a large interface roughness with increasing N is likely to cause local variation of the perpendicular anisotropy and broadening the pinning field distribution. Therefore, the observed sheared loop for trilayer films with $x_{Cr}=0.75$ nm could be attributed to the increase in local variation of in-plane anisotropy in top CoFeB262 layer with increasing y [28], which changes the nature of magnetic interaction between CoFeB262 layers. With increasing $x_{Cr}=0.75$ to 2 nm in trilayer films, no shearing of the loops was observed with increasing y . This could be attributed to the fact that with increasing x_{Cr} , the direct interaction between CoFeB262 layers is preferably discontinued and hence the interaction between CoFeB262 layers is majorly of magnetostatic in nature. In addition, the stray field coupling is always present in magnetic multilayers, because each ferromagnetic layer is placed in the demagnetization field of the others, which tends to align the magnetization of adjacent layers. But, the interlayer magnetostatic interaction through the stray fields at the edges of the continuous film of larger dimensions may be assumed to be weak [62,63] and hence any contribution to the net coupling from stray fields is almost negligible [45,64]. On the other hand, the Néel coupling is magnetostatic in nature, which strongly depends on the interfacial phenomena. If the surface of ferromagnetic layers has correlated roughness, then dipoles are set up at homologous protrusions and bumps at the interfaces as shown in Figure 6a. Such arrangements favor ferromagnetic alignment between the nearest magnetic layers. Therefore, the Néel coupling caused by the correlated interface roughness (Figure 6a) and magnetostatic coupling between the stray fields of domain walls (Figure 6b) play a key role on the

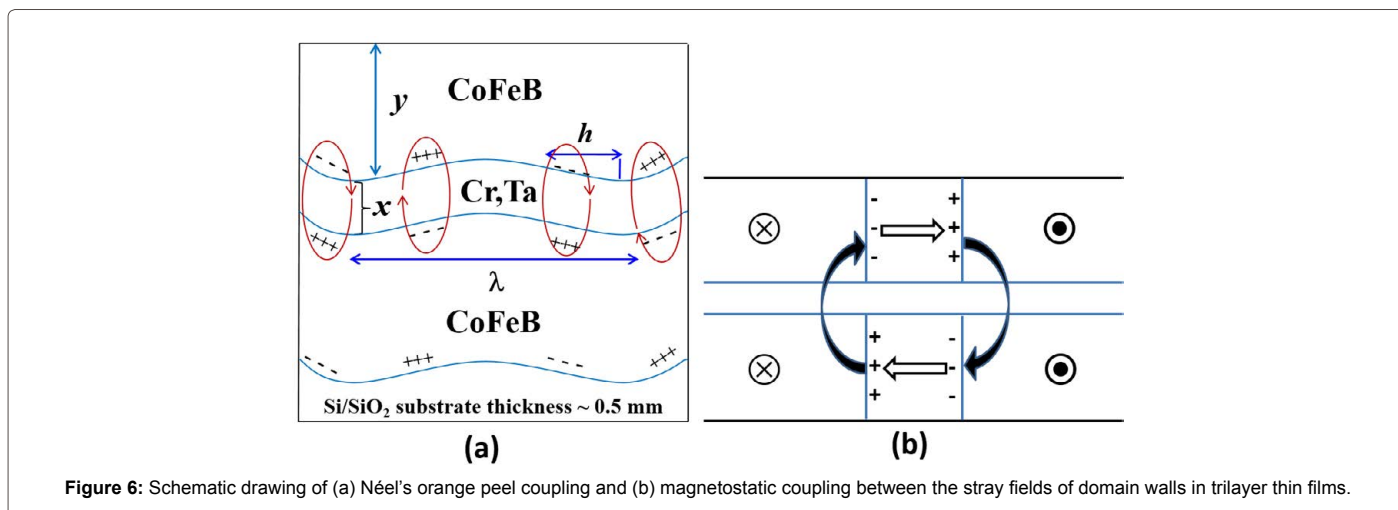


Figure 6: Schematic drawing of (a) Néel's orange peel coupling and (b) magnetostatic coupling between the stray fields of domain walls in trilayer thin films.

magnetization reversal process of the trilayer films. The magnitude of the Néel coupling field is given as [42],

$$H_C = \frac{\pi^2}{\sqrt{2}} \left(\frac{h^2}{\lambda y} \right) M_s \exp \left(-\frac{2\pi\sqrt{2}x}{\lambda} \right) \quad (1)$$

where, h and λ are the amplitude and wavelength of the interface roughness, x and y are the thicknesses of the spacer layer and top CoFeB262 layer and M_s is the saturation magnetization of the free layer respectively. The magnetostatic coupling between CoFeB262 layers disrupts the magnetic stripe domain in bottom layer and enhances the magnetic softness. Nevertheless, the magnitude of reduction in H_C decreases with increasing x_{Cr} . This could be attributed to the spacer layer thickness dependent coupling between CoFeB262 layers [42,65,66], which decreases with increasing x as given in eqn.(1). This argument also supports the results observed for trilayer films with Ta spacer layer materials, i.e., the change in the loop shape for trilayer films with $x_{Cr}=2$ nm and $x_{Ta}=1$ nm is found to be nearly the same. With increasing $x_{Ta}=4$ nm, we observed almost same type of loops for all films, which could be correlated to the reduced coupling between CoFeB262 layers through thick Ta spacer layer [8-10,29,32]. As a result, H_C reduces sluggishly as compared to all other films.

To further understand the magnetic coupling and magnetic interaction in trilayer structured films, we have investigated the magnetization reversal behavior along the film plane using MOKE microscopy. Figures 7 and 8 display the typical Kerr loops and magnetic domain images for the trilayer films with $x_{Cr}=0.75$ and $y=10$ nm and $x_{Ta}=1$ and $y=10$ nm. It is clearly evident that trilayer film with $x_{Cr}=0.75$ displays rectangular shaped loop in one direction [easy-axis direction in the plane (0°)] and nearly imprecise loop characterized by reduced remanence in another direction [hard-axis direction in the plane (90°)]. The magnetic domain images obtained along the easy-axis show a rapid switching of large-sized domains due to domain wall motion. The

magnetic field required to switch the magnetization along the easy-axis from one direction to another direction is observed to be quite low (< 5 Oe). From the VSM results (Figure 4a), the applied field required to switch the magnetization from one direction to another direction is found to be nearly 30 Oe, which is much larger than the one obtained from MOKE microscopy. This could be attributed to the contribution from the finite edge effect of the sample used in VSM measurement. On the other hand, the magnetic domain images obtained along the hard-axis reveal a weak ripple domains possibly due to an inhomogeneous local magnetic anisotropy distribution [67] caused by the interaction between CoFeB262 layers from the direct ferromagnetic coupling at random locations. For the trilayer film with $x_{Ta}=1$ nm, we have observed almost similar results along the easy-axis, i.e., a rapid switching of large-sized domains due to domain wall motion with slightly larger applied field (~ 6.2 Oe) required to switch the magnetization from one direction to another direction. However, the Kerr loop obtained along the hard-axis is found to be nearly straight line without any significant loop close to origin. Interestingly, the magnetic domain images along the hard-axis illustrate a clear coherent like rotation process, but with very faint ripple domains. These results clearly confirm that the magnetic properties of the thick CoFeB262 layers with stripe domain structure can easily be tuned in to in-plane magnetization by this simple trilayer structure concept. This is found to be much easier approach than the earlier reported methods of fabricating more number of multilayers [10,33,34].

As the magnetic properties of the films are affected by the measurement temperature, it is very much essential to understand the change in the magnetic interaction and interlayer coupling between CoFeB262 layers in trilayer films as a function of T . Therefore, $M-H$ loops are measured along the film plane at different T ranging between 30 K and 300 K for all the series of films and depicted in Figures 9 and 10 for films with x_{Cr} and x_{Ta} , respectively. $M-H$ loops obtained at different T reveal the following features: For trilayer films with $x_{Cr}=0.75$,

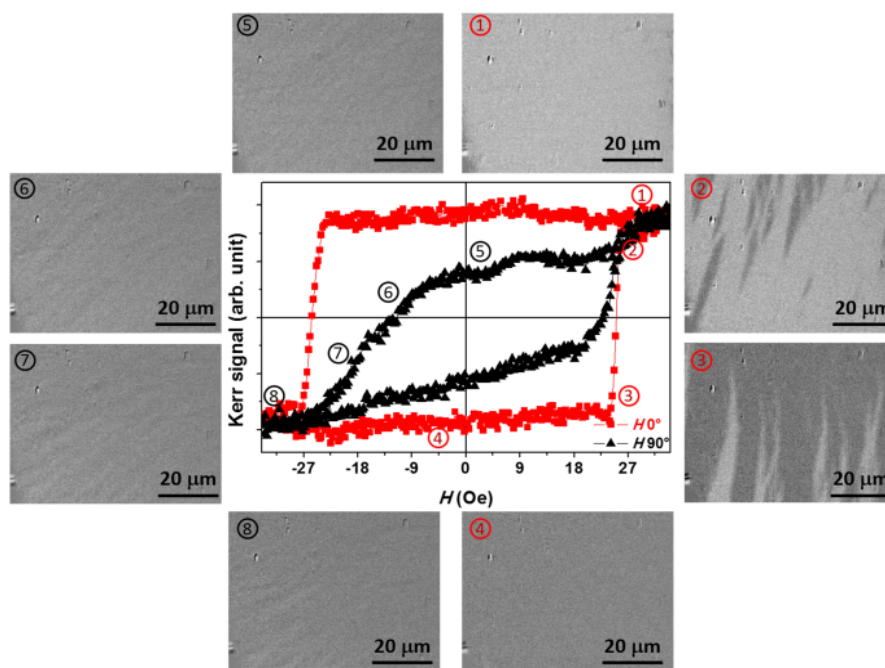


Figure 7: Room temperature Kerr loops measured along the film planes and magnetic domain images for trilayer film of [CoFeB262 (100 nm)/Cr (0.75 nm)/CoFeB262 (10 nm)].

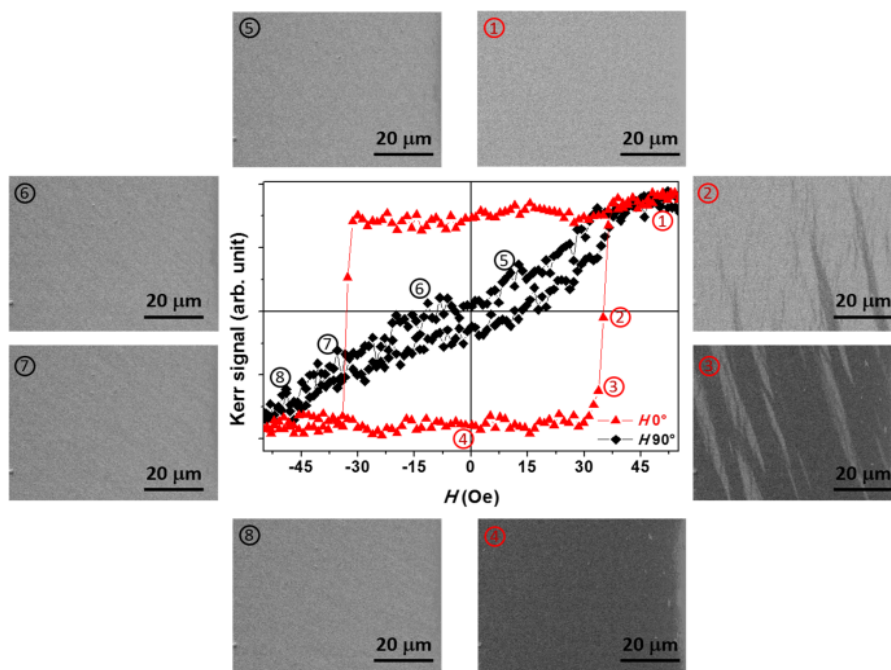


Figure 8: Room temperature Kerr loops measured along the film planes and magnetic domain images for trilayer film of [CoFeB262 (100 nm)/Ta (1 nm)/CoFeB262 (10 nm)].

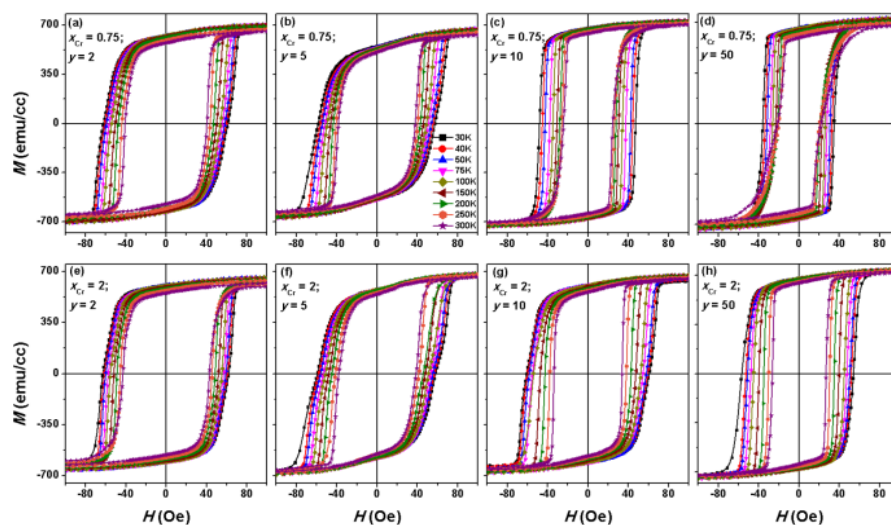


Figure 9: M - H loops measured along the film plane at different temperatures for trilayer films with different values of x_{Cr} and y .

(i) with decreasing T , the shape of the loops does not change for y up to 5 nm. However, the area under the loops increases progressively with decreasing temperature. This behavior is similar to the one observed for a typical ferromagnetic material. In addition, all the loops exhibit single magnetization reversal behavior suggesting that both top and bottom CoFeB262 layers reverse collectively at all T . (ii) With increasing $y \geq 10$, the shearing of the loop observed at room temperature diminishes with decreasing T and the loop shape turns out to be rectangular shape at T below 200 K, (iii) interestingly the temperature at which the shearing of the loop diminishes shifts to lower T with increasing y , i.e., for the film with $y=50$, the sheared loop transforms into rectangular shaped one at T below 75 K. This could be attributed to the enhanced coupling

between CoFeB262 layers as the average magnetization increases, and possibly the reduction in local variation of in-plane anisotropy in top CoFeB262 layer with decreasing T . In contrast, we have not observed any major change in the loop shape with decreasing T for films with $x_{Cr}=2$ nm and different y . Similarly, no change in the loop shapes is observed for trilayer films with $x_{Ta}=1$ nm and $y=2-50$ nm and $x_{Ta}=4$ nm and $y=2-5$. However, with increasing $y \geq 10$ nm for films with $x_{Ta}=4$ nm, we observed not only sheared loops at lower T below 50 K (Figure 10g), but also additional step like behavior before saturation, which is more pronounced with decreasing T (Figure 10h). This could be correlated to the enhanced interfacial strain for thicker films with large x , which is sensitive to the measurement T [37].

To quantitatively understand the effect of T on the magnetic parameters, the extracted values of H_C are plotted as a function of T and y in Figures 11 and 12 for films with x_{Cr} and x_{Ta} , respectively. The relative variation of H_C , i.e., $H_C(T)/H_{C@300K}$ is also plotted as a function of T for both the series as insets. H_C increases with decreasing T for all the films. However, the amount of increase in H_C depends on the values of x , y and T . For instance, the single-layer thick CoFeB262 film exhibits a non-linear variation of $H_C(T)$ and H_C varies from 47 Oe to 130 Oe with decreasing T from 300 K to 30 K. As a result, $H_C(T)/H_{C@300K}$ increases by 2.7 times. On the other hand, the variation in $H_C(T)$ decreases largely

for the trilayer films, i.e., H_C increases from 40.5, 25.4 and 20.3 Oe to 61.6, 47.6 and 35.4 Oe, respectively for the films with $x_{Cr}=0.75$ nm and $y=2, 10$ and 50 nm. Accordingly, the maximum variation of $H_C(T)/H_{C@300K}$ is found to be 1.53, 1.88, and 1.75 for the films with $x_{Cr}=0.75$ nm and $y=2, 10$ and 50 nm. On the other hand, with increasing spacer layer thickness from 0.75 to 2 nm, the variation of $H_C(T)$ for different y values diminishes, i.e., H_C increases from 42.8, 33.7, 25.2 Oe to 62.3, 60.7, 55.5 Oe, respectively for the films with $x_{Cr}=2$ nm and $y=2, 10$ and 50 nm. Similarly, the plot of H_C as a function of y at different T shows that (i) H_C decreases not only with increasing y , but also with increasing T at a

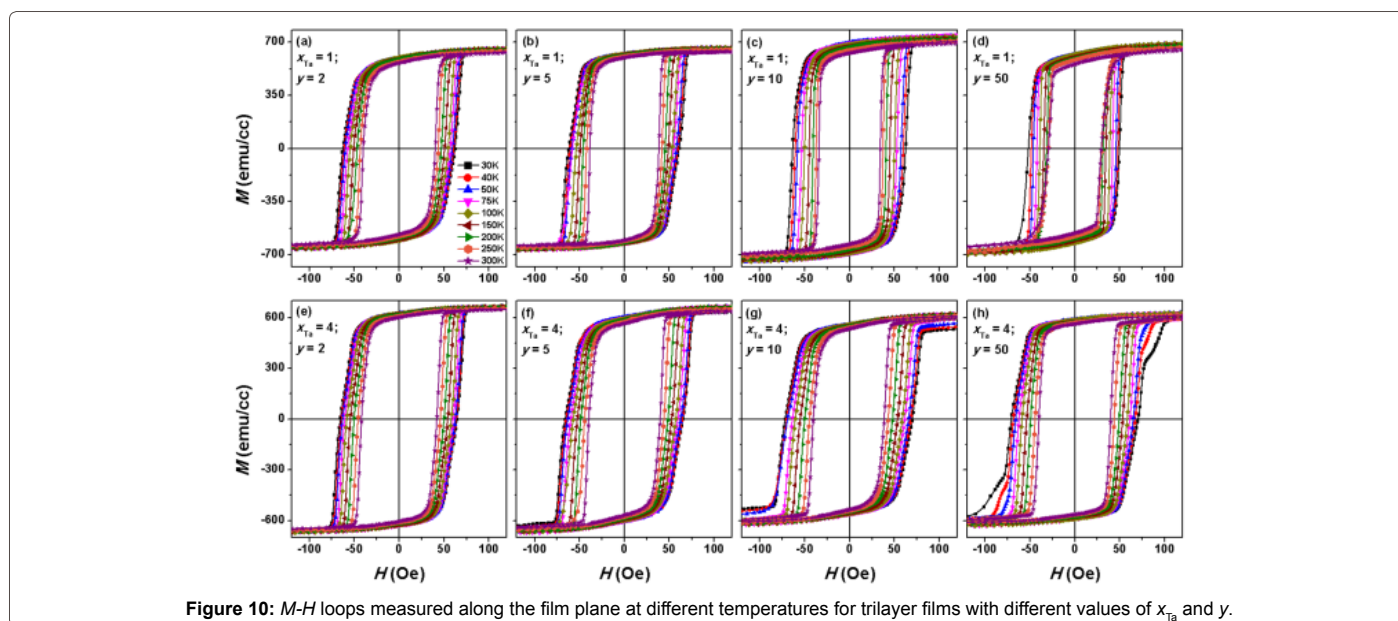


Figure 10: M - H loops measured along the film plane at different temperatures for trilayer films with different values of x_{Ta} and y .

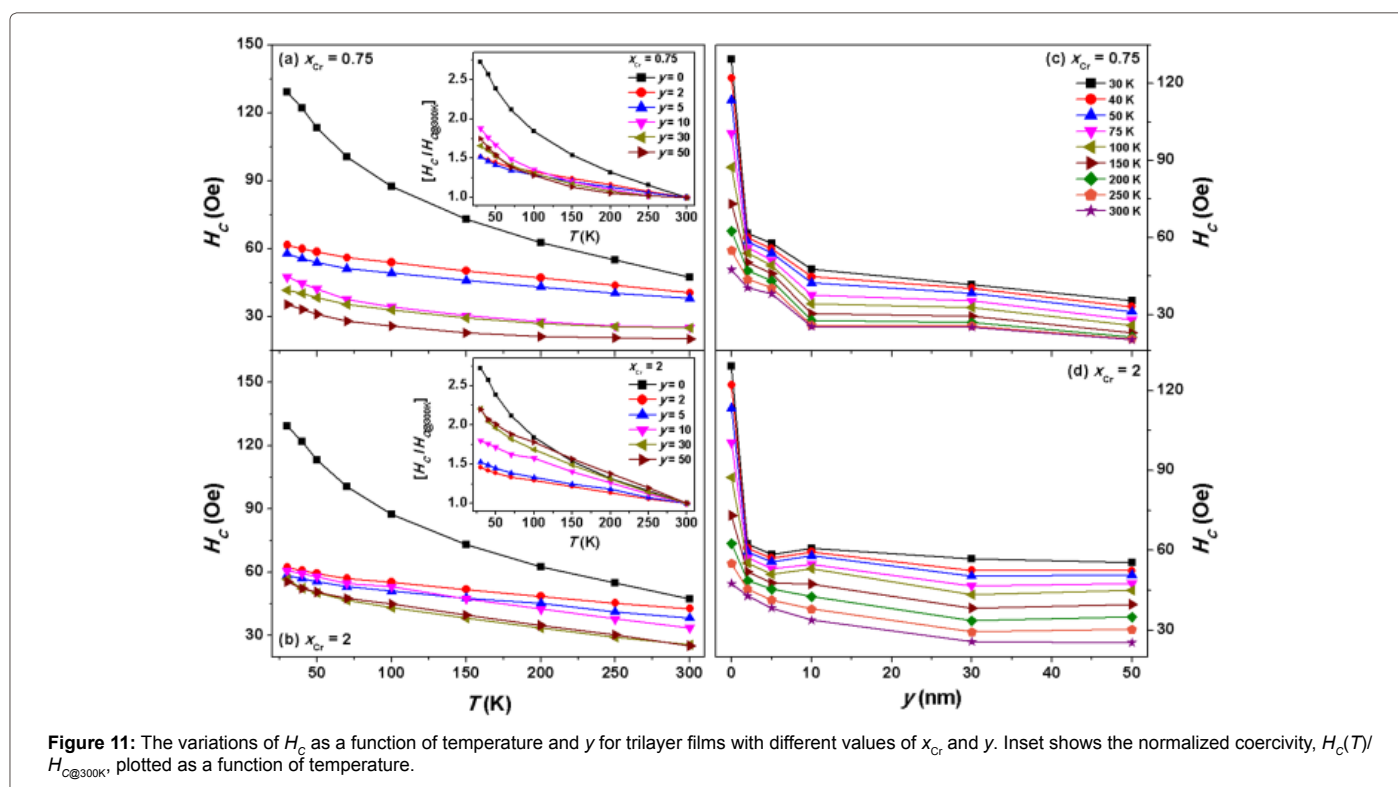


Figure 11: The variations of H_C as a function of temperature and y for trilayer films with different values of x_{Cr} and y . Inset shows the normalized coercivity, $H_C(T)/H_{C@300K}$, plotted as a function of temperature.

particular y and (ii) the amount of reduction in H_C strongly dependent on the values of x . These results suggest that with increasing T , the coupling between top and bottom CoFeB262 layers is modified due to temperature dependent magnetization and interfacial strain, which helps them to reverse faster and leads to a reduction in H_C . A similar nature of $H_C(T)$ is also observed for trilayer films with Ta spacer layer, but the relative variation in H_C is found to be nearly insensitive to y for the trilayer films with large spacer layer thickness of $x_{Ta}=4$ nm. For instance, H_C increases from 40.1, 34.1 and 29.5 Oe to 62.4, 62.9 and 50.8 Oe and from 42.1, 39.4 and 39.9 Oe to 64.9, 70.7, 70.2 Oe, respectively for the films with $x_{Ta}=1$ nm and $x_{Ta}=4$ nm with $y=2, 10$ and 50 nm. This could be attributed to the effective reduction in the interlayer coupling with increasing x .

To study $H_C(T)$ behavior in more details, $H_C(T)$ versus T curves for all the series of the films are analyzed using thermal activation effect and fitted using eqn.(2).

$$H_C(T) = H_0 \left[1 - \left(\frac{k_b T \ln(t/t_0)}{E_0} \right)^{1/\alpha} \right] \quad (2)$$

where H_0 is coercivity at zero temperature, k_b is Boltzmann

constant, E_0 is energy barrier, t is the time necessary to jump over the energy barrier at temperature T and t_0 is treated as a constant typically of the order of 10^{-9} to 10^{-11} sec. Almost all series of the data could be fitted using eqn.(2) and by taking $\alpha=2$ for T between 50 K and 300 K. However, the extension of T below 50 K shows obvious deviation of $H_C(T)$ from eqn.(2) due to larger increase in H_C at low temperatures. Considering the magnetization reversal process in these trilayer films as domain wall motion (Figures 7 and 8), the behavior of $H_C(T)$ is further analyzed using eqn.(3)

$$H_C^{1/2}(T) = H_0^{1/2} + AT^{2/3} \quad (3)$$

where H_0 is coercivity at zero temperature and A is a constant. Interestingly, H_C versus T could be fitted using eqn.(3) over the complete temperature range of 30-300 K and the extracted parameters are listed in Table 1. While the values of $H_0^{1/2}$ and A exhibit oscillatory nature with increasing y for all the films with Ta spacer layer, the variation of $H_0^{1/2}$ and A strongly depends on x_{Cr} due to different types of interaction between CoFeB262 layers in trilayer films depending on the values of x_{Cr} . These observed results suggest that temperature together with the thickness of the top CoFeB262 layer and type of spacer material has an intense effect in tuning the magnetization reversal process of

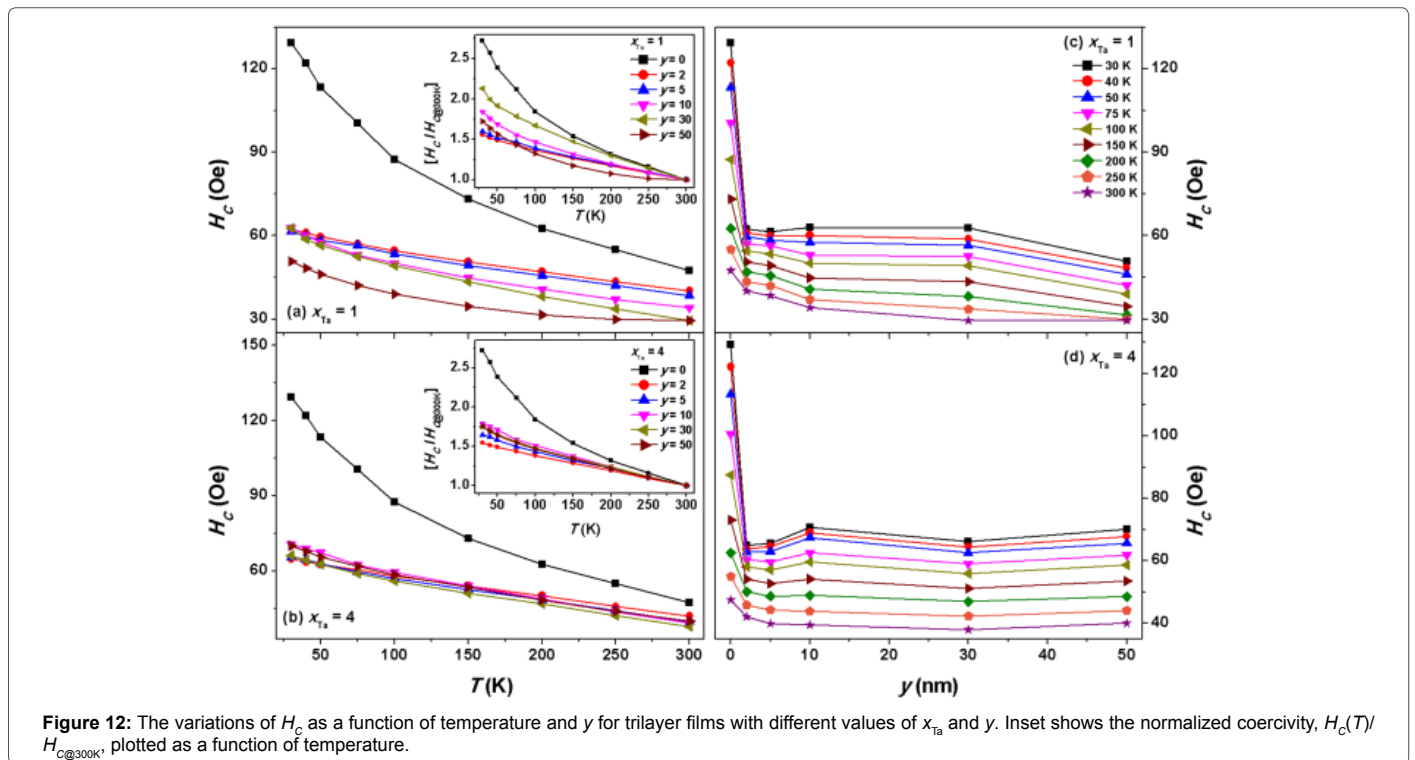


Figure 12: The variations of H_C as a function of temperature and y for trilayer films with different values of x_{Ta} and y . Inset shows the normalized coercivity, $H_C(T)/H_{C@300K}$, plotted as a function of temperature.

y	$x_{Cr}=0.75$		$x_{Cr}=2$		$x_{Ta}=1$		$x_{Ta}=4$	
	$H_0^{1/2}$ (Oe ^{1/2})	A (Oe ^{1/2} K ^{3/2})	$H_0^{1/2}$ (Oe ^{1/2})	A (Oe ^{1/2} K ^{3/2})	$H_0^{1/2}$ (Oe ^{1/2})	A (Oe ^{1/2} K ^{3/2})	$H_0^{1/2}$ (Oe ^{1/2})	A (Oe ^{1/2} K ^{3/2})
0	12.35 (4)	-0.127 (2)	12.35 (4)	-0.127 (2)	12.35 (4)	-0.127 (2)	12.35 (4)	-0.127 (2)
2	8.22 (3)	-0.041 (5)	8.24 (3)	-0.038 (2)	8.33 (3)	-0.044 (3)	8.53 (3)	-0.044 (2)
5	7.89 (2)	-0.039 (3)	8.02 (3)	-0.040 (1)	8.29 (2)	-0.046 (2)	8.62 (2)	-0.050 (4)
10	7.21 (4)	-0.054 (4)	8.39 (2)	-0.056 (2)	8.40 (2)	-0.059 (3)	9.01 (4)	-0.060 (3)
30	6.76 (3)	-0.043 (4)	8.05 (4)	-0.066 (3)	8.49 (1)	-0.068 (2)	8.67 (3)	-0.055 (3)
50	6.14 (5)	-0.041 (2)	8.04 (3)	-0.065 (2)	7.45 (3)	-0.050 (2)	8.90 (2)	-0.057 (2)

Table 1: The variation of H_0 and A for trilayer films with different spacer layer materials (x) and top CoFeB262 layer thickness (y). The number given within the parenthesis represents the error with respect to last decimal value.

thick CoFeB262 film in trilayer films. To the best of our knowledge, this is the first detailed report on tuning magnetic properties of a thick CoFeB262 film, having stripe domain structure, by fabricating simple trilayer structure and also on examining the effect of thickness of top CoFeB262 layer, different spacer material, and temperature on the resulting magnetic properties of trilayer films.

Conclusions

In the present work, we have studied the effect of trilayer structure, the spacer layer materials and its thickness (x), the thickness of top CoFeB262 layers (y) and temperature on the magnetic properties of the thick CoFeB262 films by using interlayer magnetic coupling in trilayer films of [CoFeB262 (100 nm)/Cr,Ta (x nm)/CoFeB262 (y nm)]. All the single-layer and trilayer films were deposited directly on the thermally oxidized Si substrate at ambient temperature using magnetron sputtering. The single-layer as-deposited a-CoFeB262 (100 nm) film exhibited magnetic stripe domain and transcritical hysteresis loop due to large effective magnetic anisotropy caused by the stress induced during deposition of the films at a higher deposition rate to form amorphous structure. Interestingly, the shape of magnetic hysteresis (M - H) loops in trilayer films transformed from transcritical loop to rectangular shaped one with enhanced remanence ratio (M_R/M_S) of more than 75% and single magnetization reversal behavior at coercivity (H_C). As a result, coercivity (H_C) and field required to saturate magnetization (H_S) reduced significantly in trilayer films. Nevertheless, the changes in the loop shape and reductions in H_C and H_S depend strongly on the values of x and y . Magnetic domain images obtained using Kerr microscopy in trilayer films showed rapid switching of large-sized domains along the easy-axis and weak ripple domains along the hard-axis. In addition, the nature of magnetic domains along the hard-axis strongly depend on $x_{(Cr,Ta)}$. M - H loops obtained at different low temperatures revealed almost no change in the loop shape for trilayer films with small values x and y . However, the disappearance of shearing in the loop shape and formation of additional steps at low temperatures were observed for trilayer films with large values of x and y . The temperature dependent H_C could be well fitted over the entire temperature range by considering the magnetization reversal process in these trilayer films as domain wall motion. The observed results were explained on the basis of change in interlayer coupling between CoFeB262 layers with x , y and T . Furthermore, the obtained results clearly confirmed that the magnetic properties of thick CoFeB262 films with stripe domain could easily be tuned in to in-plane magnetization by this simple trilayer films.

Acknowledgement

This work is financially supported by the Department of Science and Technology (DST), New Delhi through Science and Engineering Research Board (SR/S2/CMP/0128/2012). Infrastructure facilities provided by DST, New Delhi [SR/S2/CMP-19/2006, SR/FST/PII-020/2009] and DRDO, New Delhi [ERIP/ER/0900363/M/01/1185] are gratefully acknowledged.

References

1. Varvaro G, Casoli F (2016) Ultra-high-density magnetic recording: storage materials and media designs. CRC Press, Taylor and Francis Group, Florida.
2. Chitchekanova A, Wolf SA, Idzerda Y (2013) Magnetic interactions and spin transport. Springer Science and Business Media, New York.
3. Chen CW (2013) Magnetism and Metallurgy of Soft Magnetic Materials. (1stedn), Dover Publications, USA.
4. Kazimierczuk MK (2009) High-Frequency Magnetic Components. (2ndedn) Wiley, UK.
5. Piramanayagam SN (2007) Perpendicular recording media for hard disk drives. J Appl Phys 102: 2.

6. Mapps DJ, Akhter MA, PanG (1991) CoNbFe soft magnetic thin-film backlayers for glass computer disks. J Appl Phys 69: 5178-5180.
7. Nakagawa S, Suemitsu K, Naoe M (1997) Preparation of soft magnetic and thermally stable Fe-Co-Ta:N/Ti multilayered films by sputter deposition. J Appl Phys 81: 3782-3784.
8. Naoe M, Matsumiya H, Ichihara T, Nakagawa S (1998) Preparation of soft magnetic films of nanocrystalline Fe-Cu-Nb-Si-B alloy by facing targets sputtering. J Appl Phys 83: 6673-6675.
9. Nakamura F, Hikosaka T, Tanaka Y (2001) Low noise multi-layered FeAlSi soft magnetic films for perpendicular magnetic recording media. J Magn Magn Mater 235: 64-67.
10. Huang MQ, Hsu YN, McHenry E, Laughlin DE (2001) Soft magnetic properties of nanocrystalline amorphous HITPERM films and multilayers. IEEE Trans. Magn. 37: 2239-2241.
11. Tanahashi K, Kikukawa A, Takahashi Y, Hosoe Y (2003) Laminated nanocrystalline soft underlayers for perpendicular recording. J Appl Phys 93: 6766-6768.
12. Li XW, Song C, Yang J, Zeng F, Geng K, et al. (2007) Thickness-dependent magnetization reversal in CoZrNb amorphous films. J Magn Magn Mater 315: 120-125.
13. Coisson M, Celegato F, Olivetti E, Tiberto P, Vinai F, et al. (2008) Stripe domains and spin reorientation transition in $Fe_{78}B_{13}Si_9$ thin films produced by rf sputtering. J Appl Phys 104: 33902.
14. Singh AK, Kisan B, Mishra D, Perumal A (2012) Thickness dependent magnetic properties of amorphous FeTaC films. J Appl Phys 111: 93915.
15. Ikeda S, Miura K, Yamamoto H, Mizunuma K, Gan HD, et al. (2010) A perpendicular-anisotropy CoFeB-MgO magnetic tunnel junction. Nature Materials 9: 721-724.
16. Mantovan R, Lamperti A, Tallarida G, Baldi L, Mariani M, et al. (2013) Perpendicular magnetic anisotropy in Ta/CoFeB/MgO systems synthesized on treated SiN/SiO₂ substrates for magnetic memories. Thin Solid Films 533: 75-78.
17. Wang Y, Wei D, Gao KZ, Cao J, Wei F (2014) The role of inhomogeneity of perpendicular anisotropy in magnetic properties of ultra thin CoFeB film. J Appl Phys 115: 53901.
18. Lee SE, Baek JU, Park JG (2017) Highly Enhanced TMR Ratio and Δ for Double MgO-based p-MTJ Spin-Valves with Top Co₂Fe₂B₂ Free Layer by Nanoscale-thick Iron Diffusion-barrier. Scientific Reports 7: 11907.
19. Liu Y, Hao L, Cao J (2016) Effect of annealing conditions on the perpendicular magnetic anisotropy of Ta/CoFeB/MgO multilayers. AIP Advances 6: 45008.
20. Tomczak Y, Lin T, Swerts J, Couet S, Mertens S, et al. (2016) Influence of the Reference Layer Composition on the Back-End-of-Line Compatibility of Co/Ni-Based Perpendicular Magnetic Tunnel Junction Stacks. IEEE Trans. Magn. 52: 1-4.
21. Su L, Zhang Y, Klein JO, Zhang Y, Bourmel A, et al. (2015) Current-limiting challenges for all-spin logic devices. Scientific Reports 5: 14905.
22. Sato H, Enobio ECI, Yamanouchi M, Ikeda S, Fukami S, et al. (2014) Properties of magnetic tunnel junctions with a MgO/CoFeB/Ta/CoFeB/MgO recording structure down to junction diameter of 11 nm. Appl Phys Lett 105: 62403.
23. Liang SH, Zhang TT, Barate P, Frougier J, Vidal M, et al. (2014) Large and robust electrical spin injection into GaAs at zero magnetic field using an ultrathin CoFeB/MgO injector. Phys Rev B 90: 85310.
24. Thomas L, Jan G, Zhu J, Liu H, Lee YJ, et al. (2014) Perpendicular spin transfer torque magnetic random access memories with high spin torque efficiency and thermal stability for embedded applications. J Appl Phys 115: 172615.
25. Gajek M, Nowak JJ, Sun JZ, Trouilloud PL, O'Sullivan EJ, et al. (2012) Spin torque switching of 20 nm magnetic tunnel junctions with perpendicular anisotropy. Appl Phys Lett 100: 132408.
26. Naik VB, Meng H, Sbiaa R (2012) Thick CoFeB with perpendicular magnetic anisotropy in CoFeB-MgO based magnetic tunnel junction. AIP Advances 2: 42182.
27. Kippen L, Fulara H, Raju M, Chaudhary S (2012) In-plane magnetic anisotropy and coercive field dependence upon thickness of CoFeB. J Magn Magn Mater 324: 3118-3121.

28. Gayen A, Prasad GK, Mallik S, Bedanta S, Perumal A (2017) Effects of composition, thickness and temperature on the magnetic properties of amorphous CoFeB thin films. *J Alloys Compd* 694: 823-832.
29. Singh AK, Mallik S, Bedanta S, Perumal A (2013) Spacer layer and temperature driven magnetic properties in multilayer structured FeTaC thin films. *J Phys D: Appl Phys* 46: 445005.
30. Daniil M, Knipling KE, Fonda HM, Willard MA (2014) Non-equilibrium materials design: a case study of nanostructured soft magnets for cryogenic applications. *New J Phys* 16: 055016.
31. Feng YC, Laughlin DE, Lambeth DN (1994) Magnetic properties and crystallography of double-layer CoCrTa thin films with various interlayers. *IEEE Trans Magn* 30: 3960-3962.
32. Feng YC, Laughlin DE, Lambeth DN (1995) Multilayer CoCrTa thin film media with Cr or Ag interlayers. *IEEE Trans Magn* 31: 2845-2847.
33. Mishra D, Singh AK, Shyni PC, Sharma D, Perumal A (2011) Enhanced soft magnetic properties in multilayer structured amorphous Fe-Ta-C films. *J Appl Phys* 109: 07A304.
34. Das C, Alagarsamy P (2018) Tuning the magnetic properties of stripe domain structured CoFeB films using stack structure with spacer layer thickness dependent interlayer coupling. *J Magn Magn Mater* 448: 23-30.
35. Park JH, Park C, Jeong T, Moneck MT, Nufer NT, et al. (2008) CoPt multilayer based magnetic tunnel junctions using perpendicular magnetic anisotropy. *J Appl Phys* 103: 07A917.
36. Navas D, Redondo C, Badini Confalonieri GA, Batallan F, Devishvili A, et al. (2014) Domain-wall structure in thin films with perpendicular anisotropy: Magnetic force microscopy and polarized neutron reflectometry study. *Phys Rev B* 90: 54425.
37. Singh AK, Mallik S, Bedanta S, Perumal A (2014) Effect of Postannealing and Multilayer Structure on Soft Magnetic Properties of FeTaC Thin Film. *IEEE Trans Magn* 50: 1-4.
38. Pitcher PG, Miller J, Pearson DPA, Gurney PD (1993) Stacked Pt/Co Multilayers with Independent Control of Coercivity and Curie Temperature. *J Magn Soc Jpn* 17: S1_95-98.
39. Gusenbauer C, Ashraf T, Stangl J, Hesser G, Plach T, et al. (2011) Interdiffusion in Heusler film epitaxy on GaAs(001). *Phys Rev B* 83: 35319.
40. Singh AK, Perumal A (2016) Interlayer coupling dependent magnetic properties in amorphous and nanocrystalline FeTaC based multilayer thin films. *J Phys D: Appl Phys* 49: 85001.
41. Hubert A, Schafer R (1998) *Magnetic Domains: the Analysis of Magnetic Microstructures*. Springer-Verlag, Berlin, Heidelberg.
42. Schrag BD, Anguelouch A, Ingarvsson S, Xiao G, Lu Y, et al. (2000) Néel "orange-peel" coupling in magnetic tunneling junction devices. *Appl Phys Lett* 77: 2373-2375.
43. Chopra HD, Yang DX, Chen PJ, Parks DC, Egelhoff WF (2000) Nature of coupling and origin of coercivity in giant magnetoresistance NiO-Co-Cu-based spin valves. *Phys Rev B* 61: 9642-9652.
44. Chopra HD, Sullivan MR, Ludwig A, Quandt E (2005) Magnetoelastic and magnetostatic interactions in exchange-spring multilayers. *Phys Rev B* 72: 54415.
45. Baltz V, Marty A, Rodmacq B, Dieny B (2007) Magnetic domain replication in interacting bilayers with out-of-plane anisotropy: Application to Co/Pt multilayers. *Phys Rev B* 75: 14406.
46. Nistor LE, Rodmacq B, Auffret S, Schuhl A, Chshiev M, et al. (2010) Oscillatory interlayer exchange coupling in MgO tunnel junctions with perpendicular magnetic anisotropy. *Phys Rev B* 81: 220407.
47. Sharma P, Kimura H, Inoue A, Arenholz E, Guo J-H (2006) Temperature and thickness driven spin-reorientation transition in amorphous Co-Fe-Ta-B thin films. *Phys Rev B* 73: 52401.
48. Chen YT, Hsieh WH (2013) Thermal, magnetic, electric, and adhesive properties of amorphous Co₆₀Fe₂₀B₂₀ thin films. *J Alloys Compd* 552: 283-288.
49. Cho MH, Ko DH, Choi YG, Jeong K, Lyo IW, et al. (2001) Structural and electrical characteristics of Y₂O₃ films grown on oxidized Si(100) surface. *J Vac Sci Technol A* 19: 192-199.
50. Sun ZG, Kuramochi H, Mizuguchi M, Takano F, Semba Y, et al. (2004) Magnetic properties and domain structures of FeSiB thin films. *Surf Sci* 556: 33-38.
51. Coisson M, Vinai F, Tiberto P, Celegato F (2009) Magnetic properties of FeSiB thin films displaying stripe domains. *J Magn Magn Mater* 321: 806-809.
52. Craus CB, Chezan AR, Siekman MH, Lodder JC, Boerma DO, et al. (2002) Stripe domains in Fe-Zr-N nanocrystalline films. *J Magn Magn Mater* 240: 423-426.
53. Porrati F (2002) Spatially varying magnetic anisotropies in ultrathin films. Martin Luther University of Halle-Wittenberg.
54. Pong PWT, Dennis CL, Castillo A, Chen A, Egelhoff WF (2008) Detection of pinholes in magnetic tunnel junctions by magnetic coupling. *J Appl Phys* 103: 07A902.
55. Kudrnovsky J, Drchal V, Bruno P, Turek I, Weinberger P (1997) Interlayer exchange coupling: Effect of the cap. *Phys Rev B* 56: 8919-8927.
56. Zhang J, White RM (1996) Topological coupling in magnetic multilayer films. *J Appl Phys* 79: 5113.
57. Alvarez-Prado LM (2004) Micromagnetism of nanowires with low out-of plane-anisotropy. *Physica B: Condensed Matter* 343: 241-246.
58. Riet EV, Klaassens W, Roozeboom F (1997) On the origin of the uniaxial anisotropy in nanocrystalline soft-magnetic materials. *J Appl Phys* 81: 806-814.
59. Murayama Y (1966) Micromagnetics on Stripe Domain Films. I. Critical Cases. *J Phys Soc Jpn* 21: 2253-2266.
60. Craus CB (2003) Magnetic properties of nanocrystalline materials for high frequency applications. University of Groningen.
61. Davies JE, Hellwig O, Fullerton EE, Denbeaux G, Kortright JB, et al. (2004) Magnetization reversal of Co/Pt multilayers: Microscopic origin of high-field magnetic irreversibility. *Phys Rev B* 70: 224434.
62. Thomas L, Luning J, Scholl A, Nolting F, Anders S, et al. (2000) Oscillatory Decay of Magnetization Induced by Domain-Wall Stray Fields. *Phys Rev Lett* 84: 3462-3465.
63. Anguelouch A, Schrag BD, Xiao G, Lu Y, Trouilloud PL, et al. (2000) Two-dimensional magnetic switching of micron-size films in magnetic tunnel junctions. *Appl Phys Lett* 76: 622-624.
64. Liu XM, Ho P, Chen JS, Adeyeye AO (2012) Magnetization reversal and magnetoresistance behavior of perpendicularly magnetized [Co/Pd]_n/Au/[Co/Pd]₂ nanowires. *J Appl Phys* 112: 73902.
65. Kools JCS, Kula W, Mauri D, Lin T (1999) Effect of finite magnetic film thickness on Néel coupling in spin valves. *J Appl Phys* 85: 4466-4468.
66. Wiese N (2006) Coupling phenomena and scalability of CoFeB/Ru/CoFeB sandwiches. Bielefeld University, Germany.
67. Nowak J, Wenda J (1993) Magnetization processes and susceptibility in amorphous FeBSi films. *J Magn Magn Mater* 124: 119-127.